Article

Reactivity Ratios and Surface Properties of Confined and Bulk ATRP Copolymerization of Butyl Methacrylate and 2-Hydroxyethyl Acrylate

Laia León-Boigues, Catalina von Bilderling, Lía Pietrasanta, Omar Azzaroni, Carmen Mijangos,* and Juan M. Giussi*

Read Online

ACCESS | Metrics & More | Article Recommendations | SI Supporting Information

ABSTRACT: Tunable hardness materials have shown fascinating properties, which place them as potential materials for use in different technological fields. This work deals with the bulk and confined synthesis of copolymers based on butyl methacrylate and 2-hydroxyethyl acrylate (HEA), prepared by atom transfer radical copolymerization in the entire composition range using conventional and anodic aluminum oxide (AAO) reactors, respectively. In each case, reactivity ratios and molecular weights were calculated using nuclear magnetic resonance, and the latter were compared to the values obtained by size exclusion chromatography. Differential scanning calorimetry and thermogravimetric analysis allowed to evaluate thermal transition and decomposition profiles and, with this data, compare the differences in each system, bulk and confined. Finally, the nanostructures extracted from the AAO nanoreactor were evaluated on the surface by atomic force microscopy and the water contact angle. Interestingly, our results revealed remarkable differences in the reactivity ratios under bulk and confined conditions. Nanopolymerization increased the reactivity of the HEA monomer, and the thermal and surface analysis supported this observation. Indeed, these results will bring valuable knowledge that will advance the field of application of nanopolymeric materials as well as their potential applications in surface science.

KEYWORDS: bulk versus confined copolymerization, reactivity ratios, thermal transitions, surface properties, soft nanomaterials, tunable stiffness and wettability
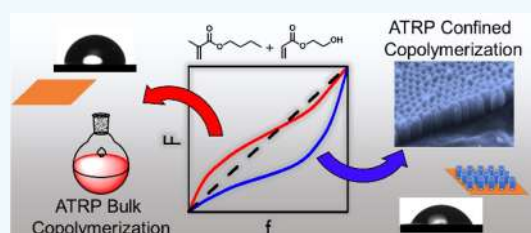
INTRODUCTION

Nanoconfined polymerization has demonstrated to be a suitable method for the creation of nanomaterials to be applied in several areas of science and technology.[1−3] The tuning features of soft nanostructured surfaces, namely, swelling capacity and rigidity, have made these surfaces an object of analysis in the fields of medicine and biology. The possibility of creating nanostructures in two dimensions integrating soft properties with the topographic features of planar substrates has allowed for the surface manipulation of certain functionalities and mechanical properties.[4,5] The interest on these nanostructured systems can be partially explained by the good interaction with cellular and biological systems.[6,7] Their physicochemical properties are responsible for these interactions, and they play a significant role on cellular adhesion, migration, proliferation, and growth.[8,9]

The possibility of transferring traditional polymerization techniques, extensively studied in bulk conditions, to confined systems, such as anodic aluminum oxide (AAO) templates, has opened a new world of exploration to create nanosystems with totally adjustable properties, thus avoiding the limitation of obtaining a nanostructured material with unexpected properties by simply nanoconfining a presynthesized polymer. The

free radical homopolymerization technique has been used to produce nanostructured polystyrene and polymethyl methacrylate.[10,11] The polymerization kinetics and the properties of the nanosystems obtained showed significant differences with respect to the bulk conditions.[12−18]

The confined space provided by porous AAO substrates has demonstrated an excellent mold to prepare polymer nanostructures with predefined morphologies.[19] Nanofibers, nanorods, and nanotubes with homo- and copolymers have been prepared by polymer infiltration using AAO templates.[20−23] In the use of AAO templates for polymer nanomolding, powdered or film polymers are infiltrated into the AAO nanopores at a high temperature for a relatively long time. During these periods of time, partial degradation of polymers can occur.[24,25] Some recent works have demonstrated that in situ polymer-

ization in AAO templates overcomes degradation issues, among other advantages.[26,27]

It is well known that controlled/"living" radical polymerization methods show several advantages over free-radical polymerization. In this sense, the possibility of using controlled methods to create nanostructured polymers using AAO substrates may be a step forward in the creation of tunable nanostructured surfaces. Atom transfer radical polymerization (ATRP)[28,29] and reversible addition–fragmentation chain-transfer polymerization[30,31] have been explored for some monomer systems in AAO templates.[32,33] Recently, Bayat et al. functionalized AAO pore templates with poly(diethylene glycol methylether methacrylate) using SI-ATRP. These authors studied the dependence of polymerization kinetics, and the degree of pore filling on the interfacial curvature was analyzed.[34]

In a previous study, with the use of free-radical copolymerization, we designed and synthesized a copolymer based on butyl methacrylate (BMA) and 2-hydroxyethyl acrylate (HEA) in only one composition under bulk and confined conditions using AAO templates.[35] The confined copolymer showed significant differences with respect to the same copolymer obtained in bulk. Molecular weight (MW), polydispersity index (PDI), Young's modulus, and wetting behavior were significantly modified. While various studies deal with HEA- and BMA-based copolymers on a separate basis, a systematic study on this monomer pair in their entire composition range is still lacking, especially the one comparing this pair behavior in the bulk versus confined condition using the same polymerization methods.

Understanding the influence of confinement on the reactivities and properties of swellable copolymers remains a key issue in the development of this type of systems. Therefore, the intention of this work was to obtain BMA- and HEA-based copolymers in their entire range of composition under bulk and confined conditions. We aimed to describe the microstructure of the BMA−HEA copolymers and to evaluate the confinement effect in the thermal and surface properties on the obtained nanostructures. To reach these goals, we used the ATRP method to copolymerize the BMA−HEA pair under bulk and confined conditions. Nuclear magnetic resonance (NMR) was used to determine the chemical composition (F_{BMA}) and molecular weight of the copolymers obtained, and the latter was compared to the values obtained by size exclusion chromatography (SEC). Differential scanning calorimetry (DSC) and thermogravimetric analysis (TGA) allowed to evaluate the thermal transition and decomposition profiles. Atomic force microscopy (AFM) and the water contact angle (WCA) were conducted to evaluate the surface properties of the nanostructures obtained.

■ MATERIALS AND METHODS

Materials. BMA (99%, contains 10 ppm monomethyl ether hydroquinone as the inhibitor) and HEA (96%, contains 200−650 ppm monomethyl ether hydroquinone as the inhibitor) monomers from Aldrich, (3-aminopropyl)triethoxysilane (APTES) (Aldrich 99%), α-bromoisobutyryl bromide (EBiB) (Aldrich, 98%), triethylamine (Aldrich, 99%), 2,2′-bipyridine (Bipy) (Anedra, 99%), and CuCl (Aldrich, 99.999%).

Copolymer Synthesis. Bulk and confined BMA−HEA copolymers in the entire composition range were synthesized by ATRP using EBiB as the initiator system and copper/Bipy as the catalyst. Below, each experimental procedure is explained.

Bulk Homo- and Copolymerization. Mixtures containing a total amount of 20 mmol of BMA_x−HEA_y were introduced into Schlenk tubes and were purged with N_2 for 30 min in an ice bath. Then, to each tube was added 0.4 mmol (62.5 mg) of Bipy, and after being purged with N_2 for 15 min, 0.2 mmol of CuCl (19.8 mg) was incorporated and the ATRP complex was formed by sonication under N_2 in an iced bath for 10 min. Finally, each tube was heated at 90 °C and 0.2 mmol of EBiB (39 mg) was introduced. After 30 min, BMA_1−HEA_0, $BMA_{0.9}$−$HEA_{0.1}$, $BMA_{0.8}$−$HEA_{0.2}$, and $BMA_{0.7}$−$HEA_{0.3}$ were precipitated into methanol and purified in two steps: dissolution in tetrahydrofuran (THF) and precipitation into methanol, centrifuged, and dried under vacuum. The more polar copolymers, $BMA_{0.3}$−$HEA_{0.7}$, $BMA_{0.2}$−$HEA_{0.8}$, and $BMA_{0.1}$−$HEA_{0.9}$, were precipitated into hexane/diethyl ether and purified with a two-step process: dissolution in THF and precipitation in hexane/diethyl ether, centrifuged, and dried under vacuum. BMA_0−HEA_1 was mixed with water and purified by dialysis and lyophilized. The absence of olefinic protons in the H NMR spectra confirmed polymer purity.

Confined Conditions. Fabrication of Anodic Aluminum Oxide Templates. Based on Masuda et al.'s[36,37] anodization method, later developed in our laboratory,[20,21] AAO templates were prepared to achieve well-ordered pore structures. The pore size and length were controlled by adjusting the synthesis parameters to obtain a well-defined geometry. The general synthesis method to obtain a pore diameter of 35 nm gazed out two electrochemical anodization processes on aluminum sheets (99,999% degree) of around 10 cm². In the first anodization process, an electropolished aluminum sheet was introduced in the electrolytic reactor with $H_2C_2O_4$ (0.3 M) and a voltage of 40 V was applied for 24 h. Then, the first alumina layer was dissolved using a phosphoric acid (H_3PO_4) solution (10% wt) and the second anodization process was performed using the same electrolyte. The anodizing time determines the pore length. Templates with an initial pore diameter of 35 nm were widened until 60 nm, in a third step, by immersing in a phosphoric acid (H_3PO_4) solution (5% wt) at 35 °C for 25 min. AAO templates were prepared with a 60 nm pore diameter and 1 and 100 μm pore lengths.

ATRP Initiator on the AAO Template (Scheme 1). The AAO substrates were first modified by immersion in a solution of 2% v/v of APTES in ethanol at 40 °C for 2 h.[4] Then, the APTES-modified substrates were washed with ethanol and cured in an oven at 150 °C for 1 h. Said substrates were then introduced in a solution of 25 mM α-bromo isobutyryl bromide (containing triethylamine, also in a concentration of 25 mM) in superdry THF under N_2 at room temperature overnight. The activated substrates were washed with THF and dried under a stream of N_2.

Copolymerization (Scheme 1). ATRP copolymerization reactions were carried out as previously reported.[4,5] Each 10 mmol of BMA_x−HEA_y ($BMA_{0.9}$−$HEA_{0.1}$, $BMA_{0.8}$−$HEA_{0.2}$, $BMA_{0.7}$−$HEA_{0.3}$, $BMA_{0.3}$−$HEA_{0.7}$, $BMA_{0.2}$−$HEA_{0.8}$, and $BMA_{0.1}$−$HEA_{0.9}$) monomer mixture was introduced into a Schlenk tube (tube 1). The mixture was purged with N_2 bubbles at 0 °C for 30 min, and then, 0.2 mmol (31.25 mg) of Bipy was incorporated. The purge was then continued for 15 min more. Afterward, 0.1 mmol of CuCl (9.9 mg) was introduced, and the mixture was sonicated under N_2 in an iced bath for 10 min. Simultaneously, each AAO substrate was sealed in a Schlenk tube (tube 2) and five vacuum/nitrogen cycles of 10 min each were carried out. The mixture of tube 1 was then quickly transferred to tube 2 via a syringe under N_2. Each polymerization was conducted at 90 °C for 30 min, and then, the substrate was removed, washed, and sonicated with toluene and ethanol and dried with N_2. The substrate was removed by two steps: first, dissolving the alumina with a mixture of HCl, $CuCl_2$, and H_2O and finally removing the aluminum with a solution of 10% wt of H_3PO_4.

Identification and Characterization. Nanoreactors, bulk copolymers, and nanostructured copolymers were characterized by different techniques and subjected to different treatments depending on the equipment used.

Scanning Electron Microscopy. The AAO templates used as nanoconfined reactors were morphologically characterized by scanning electron microscopy (SEM) (Philips XL30).

Nuclear Magnetic Resonance. After the reaction, the bulk homo- and copolymers obtained were dissolved in DMSO-d_6 (BMA$_0$−HEA$_1$ and BMA$_{0.1}$−HEA$_{0.9}$, BMA$_{0.2}$−HEA$_{0.8}$, BMA$_{0.3}$−HEA$_{0.7}$) or chloroform-d (BMA$_{0.7}$−HEA$_{0.3}$ and BMA$_{0.8}$−HEA$_{0.2}$, BMA$_{0.9}$−HEA$_{0.1}$, BMA$_1$−HEA$_0$). Then, the solution was directly taken to the equipment for analysis. Regarding the copolymers obtained under confinement, the AAO substrate was first dissolved in a minimum volume of the aqueous phosphoric acid solution and extracted with chloroform (three times). The three organic extracts (containing the copolymers) were mixed, the solvent was evaporated to dryness, and the isolated copolymers were redissolved in deuterated solvents (DMSO-d_6 or chloroform-d).

Size Exclusion Chromatography. The average molecular weight and molecular weight distribution of bulk copolymers were determined by SEC using a series of four μ-Styragel columns (10^5, 10^4, 10^3, 100 Å pore size). The polymer concentration was 5 mg/mL, and the flow rate was 0.5 mL/min. THF was used as a solvent and an eluent, and the detection method used was infrared absorption at 5.75 μm using a Miram IA spectrophotometer detector. The calibration was done using polymethyl methacrylate standards.

Differential Scanning Calorimetry. The copolymers, both bulk and confined, were characterized by DSC in a TA Instruments Q2000 DSC. All experiments were carried out in a nitrogen atmosphere by heating and cooling at 10 °C/min from −40 to 80 °C, with a previous treatment erasing thermal history. Tg values were calculated at the onset point. To analyze the copolymers in confinement, the aluminum was removed previously with an aqueous solution of CuCl$_2$ and HCl, and then, the alumina template was washed with water and dried under vacuum before being introduced into the DSC.

Thermogravimetry Analysis. A thermal stability study was carried out using TA Instruments TGA Q500. To conduct the TGA assay, the samples were subjected to a temperature ramp from 40 to 600 °C at 10 °C/min.

Atomic Force Microscopy. AFM measurements were performed under a nitrogen or aqueous (Milli-Q) environment using MultiMode 8 AFM (NanoScope V Controller, Bruker, Santa Barbara, CA). Peak force tapping (PeakForce-Quantitative NanoMechanics, PF-QNM) was used as the mapping mode. ScanAsyst-air (0.4 N/m cantilever nominal spring constant) and SNML (0.07 N/m cantilever nominal spring constant) for dry and liquid measurements were used, respectively. The thermal tune method was employed for elasticity measurements,[38] and the deflection sensitivity was determined using freshly cleaved mica as a stiff reference material. The tip shape was estimated using the blind estimation method with a titanium roughness sample (Bruker). The observed radius of the curvature of the tips was ∼20−30 nm. DMT modulus values were obtained from PeakForce QNM maps. Image processing and elasticity quantification were carried out using the commercial NanoScope Analysis software (Bruker). To perform the analysis of extracted free polymer nanopillars, the aluminum substrate of filled AAO samples was removed with a mixture of HCl, CuCl$_2$, and H$_2$O, and the alumina was dissolved with a solution of 10% wt H$_3$PO$_4$. Previously, in order to support the free nanostructures, a coating was placed over the template.[11]

For nanopillar diameter quantification, height profiles from 12 nanopillars were analyzed for each composition and condition. Mean values are reported and standard deviations as errors. For elasticity measurements, the spring constants of the cantilevers were calculated for each experiment using the thermal tune method,[38] and the deflection sensitivity was determined using freshly cleaved mica as a stiff reference material. The tip shape was estimated using the blind estimation method with a titanium roughness sample (Bruker). The observed radius of the curvature of the tips was ∼20−30 nm. DMT modulus values were obtained from PeakForce QNM maps. The significance of the difference between the two populations was evaluated using a two-sample Student's t-test ($p < 0.05$).

Image processing and elasticity quantification were carried out using the commercial NanoScope Analysis software (Bruker).

Contact Angle Measurements. Contact angle measurements were carried out using a Rame-Hart contact angle system (model 290). In a typical measurement, 0.75 μL droplet of water was deposited on the sample surface. The average contact value was obtained at five different positions of the same sample. To perform the analysis of extracted free polymer nanopillars, the aluminum substrate of filled AAO samples was removed with a mixture of HCl, CuCl$_2$, and H$_2$O and the alumina was dissolved with a solution of 10% wt H$_3$PO$_4$. Previously, in order to support the free nanostructures, a coating was placed over the template.[5,11]

■ RESULTS AND DISCUSSION

Nanoreactor Fabrication and Characterization. AAO nanoreactors, prepared via a two-step electrochemical anodization process, were characterized by SEM. This technique allows examining both the surface and length of the nanoreactors. Figure 1 shows SEM micrographs of the
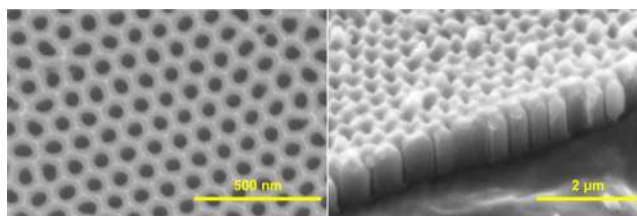
Figure 1. Front and lateral view of SEM micrographs of the synthesized AAO nanoreactors of 60 nm.

synthesized AAO nanoreactors and illustrates the obtained dimensions: around 60 nm of the pore diameter and 1 μm of the pore length. It also reveals that the nanoporosity of the nanoreactors is highly regular in size and order and that the same diameter is maintained all along the pore length.

Copolymer Synthesis and Characterization. As previously reported and in the same way aborted in this work, the chemical modification of substrates with APTES and α-bromo isobutyryl bromide produces surfaces with initiator points to be polymerized via ARPT methods.[5,32,39,40] HEA and BMA bulk homopolymerization produces homopolymers (BMA$_0$−HEA$_1$ and BMA$_1$−HEA$_0$) whose structure, H NMR spectra, and assignment of resonance signals are shown in Figure 2. Figure 3A,B displays the H NMR spectra for all bulk and confined copolymers obtained in the entire composition range.

Using the H NMR spectra of the homopolymer, in which all resonance signals had been assigned, it was then possible to assign the H NMR spectra of the copolymers.

The copolymer composition (F_{BMA}) obtained under bulk and confined conditions was estimated from the H NMR spectra (Figure 3A,B) using signals at δ = 0.7−1.05 ppm (signal e + i for the BMA monomer, corresponding to 6H) and 3.56 ppm (DMSO-d_6) or 3.79 ppm (CDCl$_3$) (signals f' for the HEA monomer, corresponding to 2H). Calculations were performed with eq 1. The change in the signal of f' from 3.56 to 3.79 ppm is due to the difference in polarity of the solvents used and the factor 3 multiplied to $I^{3.56 \text{ or } 3.79}$ is due to the integration ratio between the selected signal to the analysis, 6/2 = 3.

$$F_{BMA} = \frac{I^{0.7-1.05}}{I^{0.7-1.05} + 3 \times I^{3.56 \text{ or } 3.79}} \tag{1}$$

The number-average molecular weights (M_n) of the homo- and copolymers obtained under bulk and confined conditions were calculated using end-group analysis[41] using eq 2. Signal b, present in homo- and copolymers (under bulk and confined
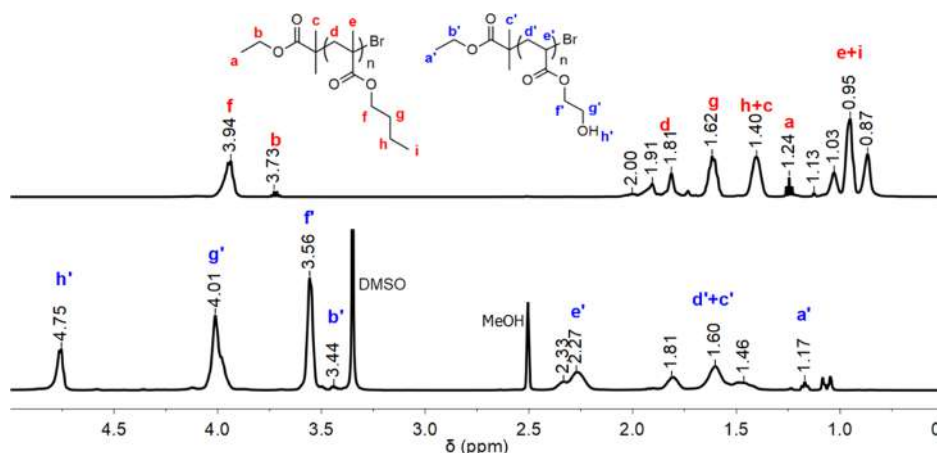
Figure 2. H NMR spectra and assignment of resonance signals of bulk homopolymers of BMA (BMA_1−HEA_0 in $CDCl_3$) and HEA [BMA_0−HEA_1 in dimethyl sulfoxide (DMSO)].
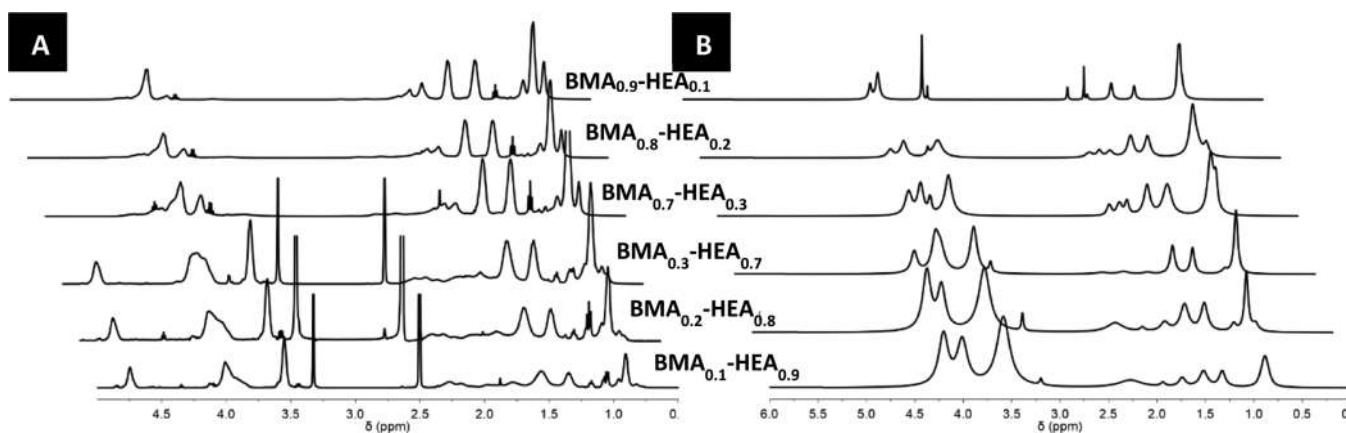
Figure 3. H NMR spectra of the copolymers obtained under bulk (A) and confined conditions (B) at 60 nm. $BMA_{0.9}$−$HEA_{0.1}$, $BMA_{0.8}$−$HEA_{0.2}$, and $BMA_{0.7}$−$HEA_{0.3}$ were measured in $CDCl_3$ and $BMA_{0.3}$−$HEA_{0.7}$, $BMA_{0.2}$−$HEA_{0.8}$, and $BMA_{0.1}$−$HEA_{0.9}$ were measured in DMSO-d_6.

conditions, see Scheme 1 to check the final confined structure proposed), was assigned as an end-group proton resonating close to 3.44 ppm in DMSO and 3.73 in $CDCl_3$.

$$M_n = \left(F_{BMA} \times M_{n\,BMA} \times \frac{I^{0.7-1.05}}{6} \right)$$
$$+ \left(F_{HEA} \times M_{n\,HEA} \times \frac{I^{3.56\ or\ 3.79}}{2} \right) + M_{n\,end\text{-}group}$$

$$(2)$$

$M_{n\,BMA}$, $M_{n\,HEA}$, and $M_{n\,end\text{-}group}$ correspond to the molecular weight of monomers and the end group, respectively. Analogous to eq 1, each molecular weight is multiplied by the corresponding weighted integration.

The number-average molecular weight (M_n) and the polydispersity indices (PDIs) for the copolymers synthesized under bulk conditions have also been determined by SEC.

Table 1 shows the bulk copolymer conversion of each mole fraction in the feed (f_{BMA}), the molar fraction in the copolymer calculated using H NMR spectra (F_{BMA}) under bulk and confined conditions, the number-average molecular weight (M_n) estimated by H NMR for bulk and confined conditions, and the number-average molecular weight (M_n) and PDI obtained by SEC for the copolymers synthesized under the bulk condition. As can be seen in the table, there are differences between the M_n values estimated by H NMR and

those obtained by SEC. According to Dwyer et al.,[42] these differences could be related to the DPn value. These authors found that for DPn values close to 1000, the deviation of the M_n values obtained by NMR and GPC is low. However, when the DPn values decrease, the deviation increases. The DPn values of the BMA−HEA system studied here are close to 50, very low enough values to produce the observed differences.

Comparison of molecular weights using NMR indicates that under bulk conditions, there is no noticeable effect of the molecular weight, while in confinement, as the fraction of BMA increases, the molecular weight decreases. This could be related to the lower interaction of the hydrophobic monomer with the template wall with respect to the hydrophilic monomer. As has already been demonstrated, a confined AAO environment usually produces a decrease in molecular weight.[10,11]

Determination of the Monomer Reactivity Ratio.
Figure 4 depicts the typical comonomer−copolymer composition curves for bulk and confined conditions. Significant differences are observed depending on the condition under analysis. Regarding the bulk condition, the curve shows a strong promotion of BMA incorporation when BMA feed is less than 0.6 ($f_{BMA} < 0.6$). HEA incorporation is increased when BMA feed is higher ($f_{BMA} > 0.6$) in the mixture. This context indicates that a copolymerization reaction proceeds statistically with an azeotropic point at a molar ratio of 0.6. If

Scheme 1. Step of BMA and HEA Copolymerization under Confined Conditions
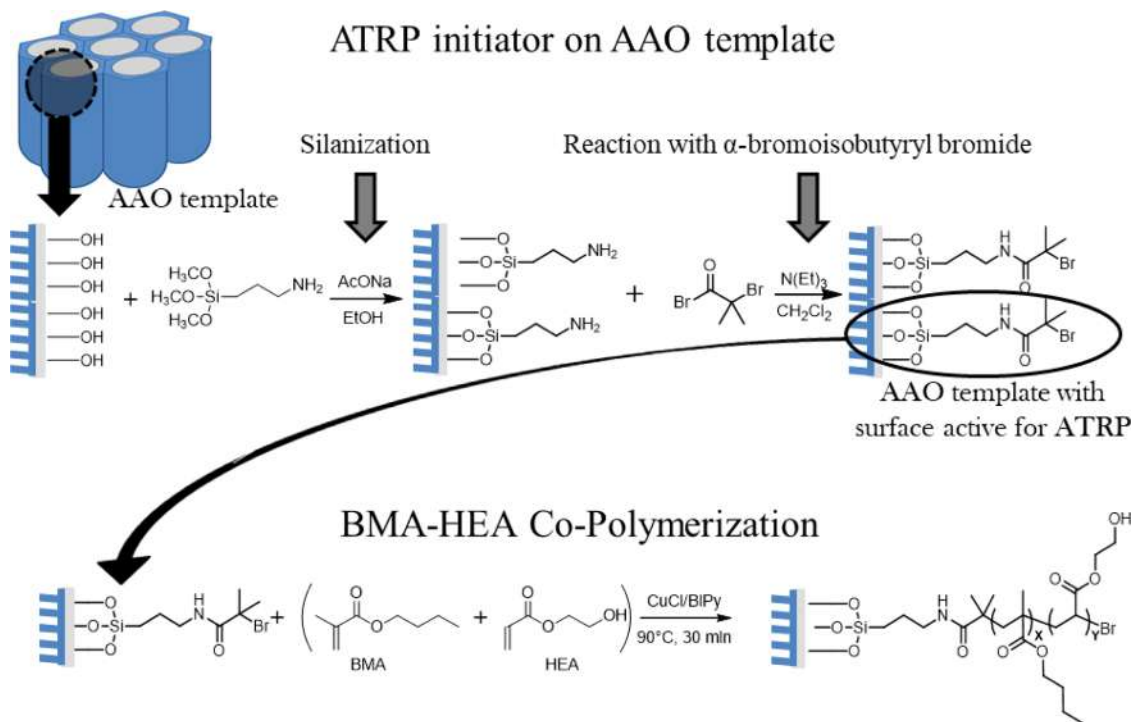
Table 1. Bulk Condition: Copolymer Conversion, BMA Monomer Mole Fraction in the Copolymer (F_{BMA}) Estimated by H NMR, Number-Average Molecular Weight (M_n) Estimated by H NMR, and Number-Average Molecular Weight (M_n) and PDI Estimated by SEC[a]

f_{BMA}	conversion (%) bulk	F_{BMA} bulk H NMR	F_{BMA} confined H NMR	M_n (g/mol) bulk H NMR	oligomers		
					M_n (g/mol) bulk SEC	PDI bulk SEC	M_n (g/mol) confined H NMR
0	3	0	0	3361			
0.1	9	0.24	0.08	2275	2464	1.21	6387
0.2	11	0.33	0.12	1870	3260	1.39	2396
0.3	12	0.43	0.21	2670	3604	1.30	1255
0.7	11	0.69	0.34	2082	6350	1.35	1446
0.8	15	0.76	0.46	2121	6595	1.23	1409
0.9	19	0.89	0.55	2329	7350	1.12	1122
1	29	1	1	3039	7264	1.15	

[a]Confined condition in 60 nm: the monomer mole fraction in the polymer (F_{BMA}) estimated by H NMR and the number-average molecular weight (M_n) estimated by H NMR.

compared to the confined copolymerization, the situation differs significantly. While the curve shows a similar profile, no azeotropic point was detected and the BMA composition in the copolymer was always smaller than that in the feed, thereby indicating that BMA has lesser reactivity.

Determining the reactivity ratios (ri) of monomer pairs allows to understand the copolymerization behavior of monomers under bulk and confined conditions. To this end, the COPOL computer software was employed.[43] This software compares values using linear and nonlinear methods, Fineman–Ross (F–R, linear method), Kelen–Tudos (K–T, linear method), Tidwell–Mortimer (T–M, nonlinear), and Lavenberg–Marqwardt (L–M, nonlinear). The mathematical theory applied in these methods is independent of the chain length, and the rate of monomer addition depends on the nature of the monomers and the growing chain end. The only requirement to apply these methods is to work at low reaction conversions (less than 20%).[44] Table 2 lists the reactivity ratios

of the monomer pairs. While the four methods provide comparable values of r_{BMA} and r_{HEA}, the nonlinear methods yielded the same values for r_{BMA} and r_{HEA} under both conditions, that is, bulk and confined. Therefore, for comparison purposes, the results from the nonlinear methods will be used. As far as the bulk condition is concerned, r_{BMA} and r_{HEA} values less than one indicate that the system copolymerizes statistically and that the azeotropic point at a molar ratio of 0.6 is due to the slightly higher reactivity of BMA than that of HEA. This is attributed to the fact that, although the reactivity values are less than 1, $r_{BMA} > r_{HEA}$ indicates the higher reactivity of the BMA monomer and the slight preference of the poly(HEA) radical for the BMA monomer ($1/r_{HEA}$ = 3.333). The product $r_{BMA} \times r_{HEA}$ = 0.198 suggests a random distribution of the monomeric units along the copolymer chain, such as the one observed for other systems. For the confined condition, the values obtained are strongly different, r_{BMA} is close to 0, while r_{HEA} is close to 1.5
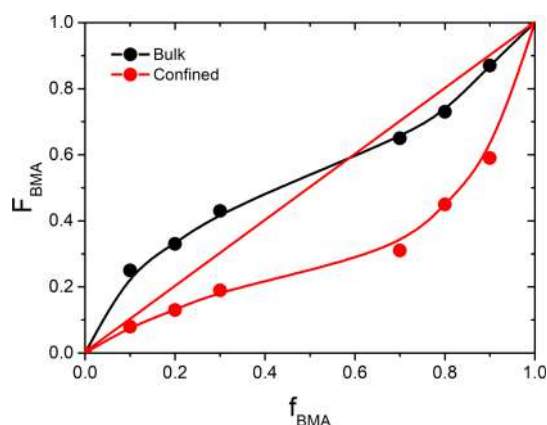
Figure 4. Copolymer composition plots for BMA and HEA monomers under bulk and confined conditions. Copolymerization carried out by ATRP with the following relative amounts (in mmoles): monomers:Bipy/CuCl/EBIB = 20:0.4:0.2:0.2 for the bulk condition and monomers/Bipy/CuCl = 10:0.2:0.1 for the confined condition in AAO with 60 nm (bromoisobutyryl initiator anchored to the nanoreactor surface). Temperature 90 °C and time = 30 min.

Table 2. Reactivity Ratios of BMA and HEA Monomer Pairs for Reactions under Bulk and Confined Conditions at 60 nm Using COPOL Software with Linear and Nonlinear Methods, F–R (Linear Method), K–T (Linear Method), T–M (Nonlinear), and L–M (Nonlinear)

	polymeric condition					
	bulk			confined		
method	r_{BMA}	r_{HEA}	correlation coefficient	r_{BMA}	r_{HEA}	correlation coefficient
F–R	0.79	0.49	0.9908	0.05	1.62	0.908
K–T	0.70	0.30	0.9877	0.01	1.32	0.955
T–M	0.66	0.30	0.9969	0.04	1.57	0.975
L–M	0.66	0.30	0.9969	0.04	1.57	0.975

($r_{BMA} < r_{HEA}$), indicating the lowest reactivity of the BMA monomer and suggesting that both types of propagating species preferentially add HEA monomers (polyBMA and polyHEA). Both monomers tend to consecutively homopolymerize. The HEA monomer, on the one hand, tends to homopolymerize until it is consumed, while the BMA monomer, on the other hand, will homopolymerize afterward. Previously, Schier and Hutchinson studied the pulsed-laser-initiated copolymerization of BMA and HEA under the bulk condition using different solvents.[45] Although without the azeotropic point, these authors found their results comparative with the results presented in this paper for the system without a solvent, r_{BMA} and r_{HEA} values less than one, and $r_{BMA} > r_{HEA}$. Based on the Tidwell–Mortimer models, the reactivity ratios obtained in this work are $r_{BMA} = 0.66$ and $r_{HEA} = 0.30$. These results are very close to the values reported by Schier and Hutchinson: $r_{BMA} = 0.98 \pm 0.13$ and $r_{HEA} = 0.37 \pm 0.09$. The introduction of solvents with donor and acceptor H-bonding capability decreases the HEA reactivity and opposite, and the introduction of nonpolar solvents increases the HEA reactivity. The differences depending on solvent characteristic are attributed to the capability of HEA to form H-bonding. In our case, in the confined condition, the reactivity of HEA substantially increases relative to that of BMA. This result could be attributed to the preconcentration effect of the HEA monomer in the wall of the template. The HEA accumulation

close to the wall is explained, considering the interaction by H-bonding between the monomer and some free Si−OH in the AAO substrate.[46]

Thermal Characterization. DSC and TGA were used to study the thermal transition and decomposition profiles of the copolymers synthesized under bulk and confined conditions. Table 3 summarizes glass transition temperatures (T_g), initial decomposition temperatures (IDTs), and temperatures of 50% degradation (TD^{50}).

Table 3. Glass Transition Temperatures (T_g), IDTs, and TD^{50} for All the Copolymers Synthesized under Bulk and Selected Copolymers Synthesized under Confined Conditions Using 60 nm Nanoreactors[a]

	bulk				confined (60 nm)			
f_{BMA}	F_{BMA}	T_g	IDT	TD^{50}	F_{BMA}	T_g	IDT	TD^{50}
0	0	−12	379	407	0			
0.1	0.24	−9	335	394	0.08	−14		
0.3	0.43	3	345	396	0.21	−6	273	359
0.7	0.69	5	326	377	0.34	7	299	362
0.9	0.89	18	308	366	0.55	−16 and 21		
1	1	20	321	371	1			

[a]DSC traces are included in the Supporting Information.

The characteristic temperatures obtained and summarized in Table 3 exhibit interesting differences for both bulk and confined conditions as a function of the copolymer composition. As expected, in bulk conditions, T_g values increase from the HEA homopolymer with a T_g of −12 °C to the BMA homopolymer with a T_g of 20 °C. As the BMA composition increases in the copolymers, the T_g values approach the BMA value, thereby suggesting a Flory−Fox behavior (eq 3) of copolymers with a statistical-alternating microstructure. As previously suggested from NMR studies, this system leads to statistical copolymers, and as a consequence, only one T_g is observed.

$$\frac{1}{T_g} = \frac{w_{BMA}}{T_{g\,BMA}} + \frac{w_{HEA}}{T_{g\,HEA}} \tag{3}$$

W_{BMA} and W_{HEA} denote the weight fractions of the respective monomers in the copolymer and T_{gBMA} and T_{gHEA} their T_g values. The T_g values of the homopolymers used in eq 2 were −12 °C for polyHEA and 20 °C for polyBMA. Figure 5 shows the experimental T_g values, along with the fit to the Flory−Fox model.

The T_g values of the copolymers fall between those of the two respective homopolymers. Glass transition arises from the onset of the backbone motions, and the order of mobility can be deduced from the T_g values of the bulk polymers. The higher the T_g, the lower the flexibility of the polymer, thus indicating that the introduction of BMA units in the polyHEA increases the rigidity of the copolymer backbone.

As far as the confined copolymers are concerned, their behavior is slightly different. Even though the tendency of T_g values seems to be dependent on the composition of the copolymer for BMA$_{0.1}$−HEA$_{0.9}$, BMA$_{0.3}$−HEA$_{0.7}$, and BMA$_{0.7}$−HEA$_{0.3}$ (with F_{BMA} of 0.08, 0.21, and 0.34, respectively), said values could not be adjusted to the Flory−Fox equation (high dispersion). It is worth noticing though that for these three cases, just one T_g value, placed between the T_g values of each
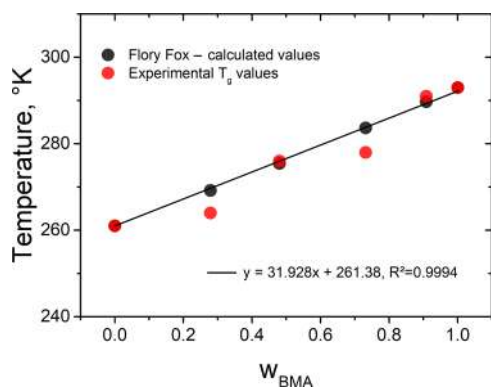
Figure 5. Experimental T_g values (red) and calculated T_g values according to Flory−Fox models (black) for bulk condition copolymerization. The lineal regression shows an R^2 value of 0.9994.

homopolymer, is observed. This suggests, once again, a statistical microstructure for these three confined copolymers. This fact does not apply to the BMA$_{0.9}$−HEA$_{0.1}$ copolymer (with an FBMA of 0.55) because two T_g values are specified under confined conditions, close to the T_g values of each homopolymer, which could suggest a more typical blocky or segmented microstructure, as shown by their reactivity relationships. These peculiar results were also reported by other authors, who suggested strong implications of nano-confinement in the values obtained.

The thermal decomposition of the synthesized copolymers is summarized in Table 3 as the initial temperature of degradation (IDT) and temperature of 50% degradation (TD^{50}). Only one thermal event was observed for all samples. Depending on both IDT and TD^{50}, the copolymers synthesized under the bulk condition yielded the following thermal stability order: BMA$_0$−HEA$_1$ > BMA$_{0.3}$−HEA$_{0.7}$ > BMA$_{0.1}$−HEA$_{0.9}$ > BMA$_{0.7}$−HEA$_{0.3}$ > BMA$_1$−HEA$_0$ > BMA$_{0.9}$−HEA$_{0.1}$. Although no clear tendency was observed, the order suggests that the increase in BMA seems to lower the thermal stability of the systems. With respect to the systems studied under confinement, such as BMA$_{0.3}$−HEA$_{0.7}$ and BMA$_{0.7}$−HEA$_{0.3}$, IDT and TD^{50} were found to be lower than those reported for the bulk condition, suggesting a priori less stability in confinement. Nonetheless, note that for composition purposes, the comparison mentioned above should be applied. Regarding the copolymer composition, based on the F_{BMA} values obtained, the confined systems BMA$_{0.3}$−HEA$_{0.7}$ and BMA$_{0.7}$−HEA$_{0.3}$ were more comparable to the BMA$_{0.1}$−HEA$_{0.9}$ and BMA$_{0.3}$−HEA$_{0.7}$ systems in bulk. Taking the forgoing comparison into account, the tendency remained the
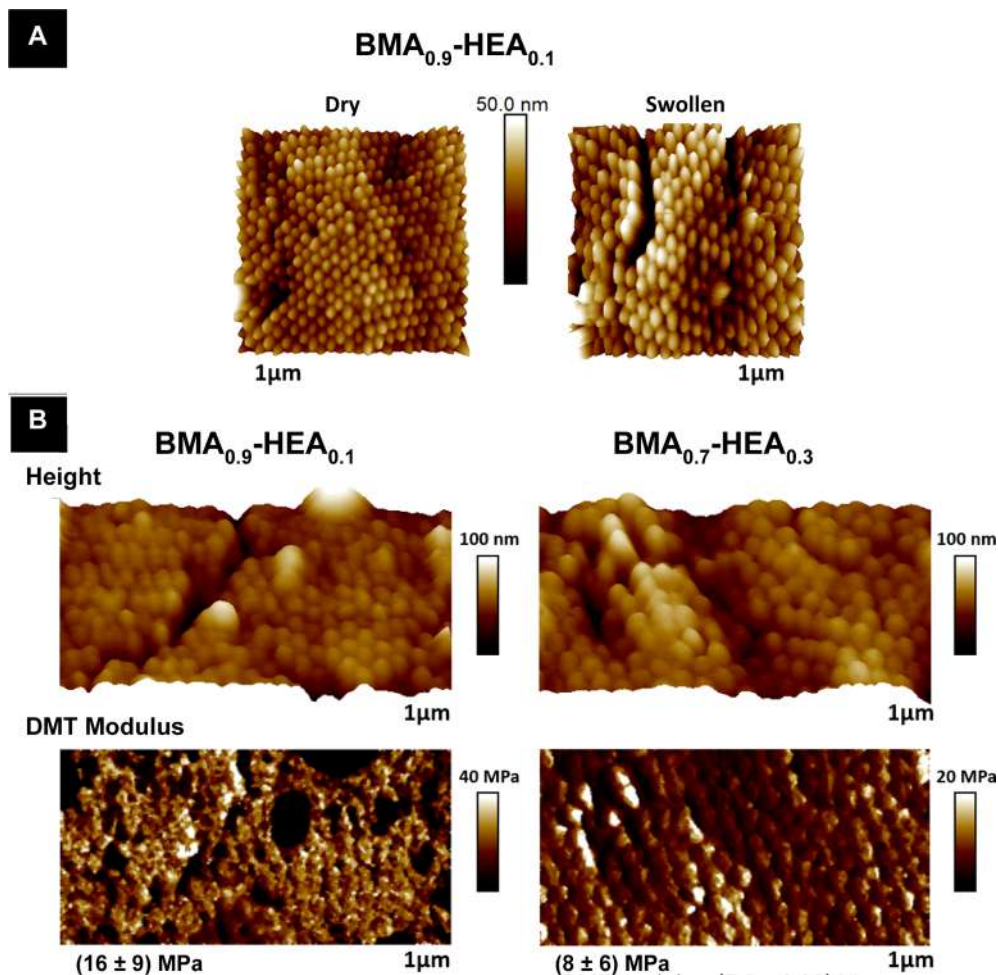
Figure 6. Nanopillar films based on BMA$_{0.9}$−HEA$_{0.1}$ and BMA$_{0.7}$−HEA$_{0.3}$ copolymers: (A) BMA$_{0.9}$−HEA$_{0.1}$ nanopillar topography AFM images (1 μm^2) obtained in a dry or aqueous environment. (B) QNM mapping of BMA$_{0.9}$−HEA$_{0.1}$ and BMA$_{0.7}$−HEA$_{0.3}$ nanopillar surfaces in topography (height) and DMT modulus channels. Mean DMT modulus values are shown for each map, with standard deviation taken as error (see Figure S3).

same for $BMA_{0.3}$–$HEA_{0.7}$ in bulk and $BMA_{0.7}$–$HEA_{0.3}$ in confinement: lower IDT and TD^{50} values were obtained as compared to $BMA_{0.3}$–$HEA_{0.7}$ in bulk and $BMA_{0.7}$–$HEA_{0.3}$ in confinement.

Nanostructure Characterization. The copolymerization of BMA and HEA in confinement by SI-ATRP produces confined copolymers that, after specific treatments (see Materials and Methods), result in nanopillar films based on BMA–HEA copolymers, as shown in Figure 6 for $BMA_{0.9}$–$HEA_{0.1}$ and $BMA_{0.7}$–$HEA_{0.3}$. AFM nanomechanical mapping was carried out on the free nanopillar surfaces of the copolymers synthesized in confinement. A composition with a higher HEA content ($BMA_{0.3}$–$HEA_{0.7}$) was also tested, but mechanical properties could not be measured because of experimental constraints (specifically, the sample elasticity was too small for the available cantilevers and the obtained force curves were not reliable for quantification). The swelling and mechanical properties of the copolymers displayed interesting differences. Figure 6A illustrates the AFM topography images ($1 \, \mu m \times 1 \, \mu m$) of the $BMA_{0.9}$–$HEA_{0.1}$ copolymer measured in a dry and aqueous environment (the sample had been kept in water before reaching the swelling equilibrium). As previously described,[35] water influence on the nanopillar sizes can be observed. The swelling effect of these nanomaterials exhibited an important size variation, as measured from vertical profiles of the AFM images. The $BMA_{0.9}$–$HEA_{0.1}$ nanopillar mean diameter increases from (61 ± 8) to (75 ± 12) nm, and the $BMA_{0.7}$–HEA_{03} (see Figure S2) nanopillar mean diameter also increases from (60 ± 5) to (72 ± 7) nm.

The mechanical properties of the nanopillar surfaces were studied by the fast force-tapping Quantitative NanoMechanics mode (QNM, Bruker). This AFM measurement mode allows for the determination of the surface topography with high resolution, as well as different mechanical properties of the sample such as the elastic modulus and adhesion in a short amount of time. It is important to mention that, as a result of the short interaction time, the absolute value of the elastic moduli obtained from this mode lacks precision. However, these measurements provide valuable high-resolution contrast maps of surface distribution of the mechanical properties, and sample elasticities can be compared if measured in the same experimental conditions.[47] Figure 6B compares high-resolution QNM images ($1 \, \mu m \times 0.5 \, \mu m$) of $BMA_{0.9}$–$HEA_{0.1}$ and $BMA_{0.7}$–$HEA_{0.3}$ copolymers measured in an aqueous environment, acquired at a 0.25 kHz tip vibration frequency. In addition to surface topography, these measurements provide a simultaneous contrast variation for regions with differences in stiffness (DMT modulus maps). As expected, the mean DMT modulus value (obtained by averaging the values from the measured maps) for $BMA_{0.9}$–$HEA_{0.1}$ (16 ± 9 MPa) was significantly ($p < 0.05$) higher than that for $BMA_{0.7}$–$HEA_{0.3}$ (8 ± 6 MPa). This difference is directly associated with the composition of the copolymer, and the increase in HEA composition decreases stiffness and enhances the softening behavior.

Finally, surface wettability also revealed interesting differences for the systems under bulk and confined conditions. In this case, films of bulk copolymers were compared to the free nanopillars of the copolymers synthesized in the confined condition. Figure 7 shows the WCA results in order to study the surface wettability for selected copolymers, $BMA_{0.3}$–$HEA_{0.7}$ and $BMA_{0.7}$–$HEA_{0.3}$. As expected, for each composition, the confined copolymer showed more hydrophilicity than

Figure 7. WCA of nanostructured surfaces (nanopillars) of $BMA_{0.3}$–$HEA_{0.7}$ and $BMA_{0.7}$–$HEA_{0.3}$ obtained under confined conditions using AAO with 60 nm. To analyze the effects separately, the final compositions of four copolymers were analyzed. For $BMA_{0.3}$–$HEA_{0.7}$ and $BMA_{0.7}$–$HEA_{0.3}$ in bulk, the final compositions were 0.43 and 0.69 in BMA, respectively, while for $BMA_{0.3}$–$HEA_{0.7}$ and $BMA_{0.7}$–$HEA_{0.3}$ in confinement, they were 0.21 and 0.34 in BMA, respectively.

its analogous in bulk. This could be attributed to two effects: composition (each system has more HEA monomers when confined than in bulk) and nanostructuration. To analyze the effects separately, the final composition of four copolymers was analyzed. For $BMA_{0.3}$–$HEA_{0.7}$ and $BMA_{0.7}$–$HEA_{0.3}$ in bulk, the final compositions for BMA in the copolymer are 0.43 and 0.69, respectively, while in confinement, they are 0.21 and 0.34, respectively. Taking into account that the final composition of BMA in the copolymer obtained from $BMA_{0.3}$–$HEA_{0.7}$ in bulk is 0.43 and that obtained from $BMA_{0.7}$–$HEA_{0.3}$ in confinement is 0.34, we assume that both compositions are close, so the variation in hydrophobicity could be attributed to the increase in the polymer's roughness in the confined system. These results are in agreement with previously reported results.[4,48,49] As can be observed, the confinement effect improves hydrophilicity following this reasoning. As demonstrated above, the nanostructuration amplified the surface characteristics, and these results are in line with the water affinity and swelling capacity of these systems. Besides, an interpenetration effect could be observed on hydrophilic surfaces. The comparison of both confined systems showed the same WCA, 58 ± 2 for $BMA_{0.3}$–$HEA_{0.7}$ and 58 ± 2 for $BMA_{0.7}$–$HEA_{0.3}$ because the final compositions are close for both systems, 0.21 and 0.34 in BMA for $BMA_{0.3}$–$HEA_{0.7}$ and $BMA_{0.7}$–$HEA_{0.3}$, respectively. Finally, and in order to consider only the final compositions without the nanostructured effect, the comparison of both bulk systems showed an increase in hydrophilicity for the system with more HEA content, $BMA_{0.3}$–$HEA_{0.7}$, with a BMA content of 0.43 (with respect to $BMA_{0.7}$–$HEA_{0.3}$ with a BMA content of 0.69).

These WCA and AFM results support the fact that in the confined condition, the reactivity of HEA substantially increases relative to that of BMA and the assumption that this could be attributed to the preconcentration effect of the HEA monomer in the wall of the template.

In summary, this work describes a comparative synthesis and characterization of copolymers based on BMA and HEA under bulk and confined conditions. The obtained results denote clear differences in the copolymerization behavior under each condition, as indicated by the reactivity ratios. These differences were supported by the thermal analysis conducted. The mechanical characteristics, wettability, and swelling properties of some nanostructured surfaces have demonstrated remarkable differences depending on the copolymer composition.

The possibility to design nanostructures from monomers (the simplest constitutive component) with predictable characteristics and properties offers an interesting platform for the design and synthesis of nanostructured soft materials.

CONCLUSIONS

The synthesis of biointeresting copolymers based on BMA and 2-hydroxyethyl acrylate was carried out under bulk and confined conditions using ATRP techniques. Important differences were detected in terms of copolymerization behavior depending on the copolymerization condition under analysis, evidenced by the reactivity ratios. The thermal characteristics, T_g values, and decomposition profiles supported these differences. The nanomechanical features of the nanostructured copolymer films obtained under confinement showed predictable differences depending on the final composition of the copolymer, that is, when HEA is increased, the monomer surface becomes softer and more hydrophilic.

This work sheds light on the design and synthesis of copolymers under different conditions and develops further understanding of the influence of these conditions in the way the system evolves. As previously demonstrated, the selected comonomer pair is an interesting system for biomedical applications. In this way, the directed construction of nanostructured biofriendly films with predictable and tunable surface properties can contribute to the development of nano- and biomedicine materials.

ASSOCIATED CONTENT

Ⓢ Supporting Information

The Supporting Information is available free of charge at https://pubs.acs.org/doi/10.1021/acsapm.0c00910.

> Tg values for bulk and confined systems, BMA0.7-HEA0.3 nanopillars QNM-topography AFM images, and mean DMT modulus values for nanopillar films (PDF)

AUTHOR INFORMATION

Corresponding Authors

Carmen Mijangos − *Instituto de Ciencia y Tecnología de Polímeros, ICTP-CSIC, 28006 Madrid, Spain;* ● orcid.org/0000-0003-3347-3181; Email: cmijangos@ictp.csic.es

Juan M. Giussi − *Instituto de Investigaciones Fisicoquímicas Teóricas y Aplicadas (INIFTA), Departamento de Química, Facultad de Ciencias Exactas, Universidad Nacional de La Plata−CONICET, 1900 La Plata, Argentina;* ● orcid.org/0000-0001-9113-9873; Email: jmgiussi@quimica.unlp.edu.ar

Authors

Laia León-Boigues − *Instituto de Ciencia y Tecnología de Polímeros, ICTP-CSIC, 28006 Madrid, Spain; Instituto de Investigaciones Fisicoquímicas Teóricas y Aplicadas (INIFTA), Departamento de Química, Facultad de Ciencias Exactas, Universidad Nacional de La Plata−CONICET, 1900 La Plata, Argentina;* ● orcid.org/0000-0002-0592-1007

Catalina von Bilderling − *Instituto de Investigaciones Fisicoquímicas Teóricas y Aplicadas (INIFTA), Departamento de Química, Facultad de Ciencias Exactas, Universidad Nacional de La Plata−CONICET, 1900 La Plata, Argentina;* ● orcid.org/0000-0002-4913-5307

Lía Pietrasanta − *Instituto de Física de Buenos Aires (IFIBA-CONICET) and Departamento de Física, Facultad de Ciencias Exactas y Naturales, Universidad de Buenos Aires, C1428EHA Buenos Aires, Argentina;* ● orcid.org/0000-0002-2714-3162

Omar Azzaroni − *Instituto de Investigaciones Fisicoquímicas Teóricas y Aplicadas (INIFTA), Departamento de Química, Facultad de Ciencias Exactas, Universidad Nacional de La Plata−CONICET, 1900 La Plata, Argentina;* ● orcid.org/0000-0002-5098-0612

Complete contact information is available at:
https://pubs.acs.org/10.1021/acsapm.0c00910

Notes

The authors declare no competing financial interest.

ACKNOWLEDGMENTS

REFERENCES

(1) Jiao, Y.; Wu, F.; Xie, A.; Wu, L.; Zhao, W.; Zhu, X.; Qi, X. Electrically Conductive Conjugate Microporous Polymers (CMPs) via Confined Polymerization of Pyrrole for Electromagnetic Wave Absorption. *Chem. Eng. J.* **2020**, *398*, 125591.

(2) Wang, T.; Sun, Y.; Zhang, L.; Li, K.; Yi, Y.; Song, S.; Li, M.; Qiao, Z. A.; Dai, S. Space-Confined Polymerization: Controlled Fabrication of Nitrogen-Doped Polymer and Carbon Microspheres with Refined Hierarchical Architectures. *Adv. Mater.* **2019**, *31*, 1807876.

(3) Chen, X.; Meng, F.; Zhou, Z.; Tian, X.; Shan, L.; Zhu, S.; Xu, X.; Jiang, M.; Wang, L.; Hui, D.; et al. One-Step Synthesis of Graphene/Polyaniline Hybrids by in Situ Intercalation Polymerization and Their Electromagnetic Properties. *Nanoscale* **2014**, *6*, 8140−8148.

(4) Sanz, B.; von Bilderling, C.; Tuninetti, J. S.; Pietrasanta, L.; Mijangos, C.; Longo, G. S.; Azzaroni, O.; Giussi, J. M. Thermally-Induced Softening of PNIPAm-Based Nanopillar Arrays. *Soft Matter* **2017**, *13*, 2453−2464.

(5) Giussi, J. M.; von Bilderling, C.; Alarcón, E.; Pietrasanta, L. I.; Hernandez, R.; del Real, R. P.; Vázquez, M.; Mijangos, C.; Cortez, M. L.; Azzaroni, O. Thermo-Responsive PNIPAm Nanopillars Displaying Amplified Responsiveness through the Incorporation of Nanoparticles. *Nanoscale* **2018**, *10*, 1189−1195.

(6) Jiang, K.; Coffer, J. L.; Akkaraju, G. R. Silicon Nanowire/Polycaprolactone Composites and Their Impact on Stromal Cell Function. *J. Mater. Res.* **2013**, *28*, 185−192.

(7) Timko, B. P.; Cohen-Karni, T.; Yu, G.; Qing, Q.; Tian, B.; Lieber, C. M. Electrical Recording from Hearts with Flexible Nanowire Device Arrays. *Nano Lett.* **2009**, *9*, 914−918.

(8) Best, J. P.; Javed, S.; Richardson, J. J.; Cho, K. L.; Kamphuis, M. M. J.; Caruso, F. Stiffness-Mediated Adhesion of Cervical Cancer Cells to Soft Hydrogel Films. *Soft Matter* **2013**, *9*, 4580.

(9) Best, J. P.; Neubauer, M. P.; Javed, S.; Dam, H. H.; Fery, A.; Caruso, F. Mechanics of PH-Responsive Hydrogel Capsules. *Langmuir* **2013**, *29*, 9814−9823.

(10) Giussi, J. M.; Blaszczyk-Lezak, I.; Cortizo, M. S.; Mijangos, C. In-Situ Polymerization of Styrene in AAO Nanocavities. *Polymer* **2013**, *54*, 6886−6893.

(11) Sanz, B.; Ballard, N.; Asua, J. M.; Mijangos, C. Effect of Confinement on the Synthesis of PMMA in AAO Templates and Modeling of Free Radical Polymerization. *Macromolecules* **2017**, *50*, 811−821.

(12) Xu, X.; Zeng, Y.; Yu, C.; Zhang, F. Controlled RAFT Polymerization of MMA in Confined Space of Various Pore Sizes of SBA-15. *J. Porous Mater.* **2020**, *27*, 95−105.

(13) Uemura, T.; Ono, Y.; Kitagawa, K.; Kitagawa, S. Radical Polymerization of Vinyl Monomers in Porous Coordination Polymers: Nanochannel Size Effects on Reactivity, Molecular Weight, and Stereostructure. *Macromolecules* **2008**, *41*, 87−94.

(14) Zhao, H.; Simon, S. L. Methyl Methacrylate Polymerization in Nanoporous Confinement. *Polymer* **2011**, *52*, 4093−4098.

(15) Zhao, H. Y.; Yu, Z. N.; Begum, F.; Hedden, R. C.; Simon, S. L. The Effect of Nanoconfinement on Methyl Methacrylate Polymerization: Tg, Molecular Weight, and Tacticity. *Polymer* **2014**, *55*, 4959−4965.

(16) Tian, Q.; Zhao, H.; Simon, S. L. Kinetic Study of Alkyl Methacrylate Polymerization in Nanoporous Confinement over a Broad Temperature Range. *Polymer* **2020**, *205*, 122868.

(17) Kalogeras, I. M.; Neagu, E. R. Interplay of Surface and Confinement Effects on the Molecular Relaxation Dynamics of Nanoconfined Poly(Methyl Methacrylate) Chains. *Eur. Phys. J. E* **2004**, *14*, 193−204.

(18) Ng, S. M.; Ogino, S.-i.; Aida, T.; Koyano, K. A.; Tatsumi, T. Free Radical Polymerization within Mesoporous Zeolite Channels. *Macromol. Rapid Commun.* **1997**, *18*, 991−996.

(19) Wu, H.; Higaki, Y.; Takahara, A. Molecular Self-Assembly of One-Dimensional Polymer Nanostructures in Nanopores of Anodic Alumina Oxide Templates. *Prog. Polym. Sci.* **2018**, *77*, 95−117.

(20) Martín, J.; Maiz, J.; Sacristan, J.; Mijangos, C. Tailored polymer-based nanorods and nanotubes by "template synthesis": From preparation to applications. *Polymer* **2012**, *53*, 1149−1166.

(21) Mijangos, C.; Hernández, R.; Martín, J. A Review On The Progress Of Polymer Nanostructures With Modulated Morphologies And Properties, Using Nanoporous Aao Templates. *Prog. Polym. Sci.* **2016**, *54−55*, 148−182.

(22) Pulamagatta, B.; Yau, M. Y. E.; Gunkel, I.; Thurn-Albrecht, T.; Schröter, K.; Pfefferkorn, D.; Kressler, J.; Steinhart, M.; Binder, W. H. Block Copolymer Nanotubes by Melt-Infiltration of Nanoporous Aluminum Oxide. *Adv. Mater.* **2011**, *23*, 781−786.

(23) Rath, A.; Theato, P. Advanced AAO Templating of Nanostructured Stimuli-Responsive Polymers: Hype or Hope? *Adv. Funct. Mater.* **2020**, *30*, 1902959.

(24) van der Spoel, D.; Lindahl, E.; Hess, B.; Groenhof, G.; Mark, A. E.; Berendsen, H. J. C. GROMACS: Fast, Flexible, and Free. *J. Comput. Chem.* **2005**, *26*, 1701−1718.

(25) Blaszczyk-Lezak, I.; Maiz, J.; Sacristán, J.; Mijangos, C. Monitoring the Thermal Elimination of Infiltrated Polymer from AAO Templates: An Exhaustive Characterization after Polymer Extraction. *Ind. Eng. Chem. Res.* **2011**, *50*, 10883−10888.

(26) Chang, C.-W.; Chi, M.-H.; Chu, C.-W.; Ko, H.-W.; Tu, Y.-H.; Tsai, C.-C.; Chen, J.-T. Microwave-Annealing-Induced Nanowetting: A Rapid and Facile Method for Fabrication of One-Dimensional Polymer Nanomaterials. *RSC Adv.* **2015**, *5*, 27443−27448.

(27) Tarnacka, M.; Chrobok, A.; Matuszek, K.; Golba, S.; Maksym, P.; Kaminski, K.; Paluch, M. Polymerization of Monomeric Ionic Liquid Confined within Uniaxial Alumina Pores as a New Way of Obtaining Materials with Enhanced Conductivity. *ACS Appl. Mater. Interfaces* **2016**, *8*, 29779−29790.

(28) Chu, C.-W.; Higaki, Y.; Cheng, C.-H.; Cheng, M.-H.; Chang, C.-W.; Chen, J.-T.; Takahara, A. Zwitterionic Polymer Brush Grafting on Anodic Aluminum Oxide Membranes by Surface-Initiated Atom Transfer Radical Polymerization. *Polym. Chem.* **2017**, *8*, 2309−2316.

(29) Guo, C.; Zhou, L.; Lv, J. Surface Initiated ATRP of Acrylic Acid on Dopamine-Functionalized AAO Membranes. *J. Appl. Polym. Sci.* **2010**, *117*, 534−541.

(30) Song, C.; Wang, M.; Liu, X.; Wang, H.; Chen, X.; Dai, L. Fabrication of High-Capacity Polyelectrolyte Brush-Grafted Porous AAO-Silica Composite Membrane via RAFT Polymerization. *Mater. Sci. Eng., C* **2017**, *78*, 748−755.

(31) Maksym, P.; Tarnacka, M.; Wolnica, K.; Dzienia, A.; Erfurt, K.; Chrobok, A.; Zięba, A.; Bielas, R.; Kaminski, K.; Paluch, M. Studies on the hard confinement effect on the RAFT polymerization of a monomeric ionic liquid. Unexpected triggering of RAFT polymerization at 30 °C. *Polym. Chem.* **2018**, *9*, 335−345.

(32) Cui, Y.; Tao, C.; Zheng, S.; He, Q.; Ai, S.; Li, J. Synthesis of Thermosensitive PNIPAM-Co-MBAA Nanotubes by Atom Transfer Radical Polymerization within a Porous Membrane. *Macromol. Rapid Commun.* **2005**, *26*, 1552−1556.

(33) Yameen, B.; Kaltbeitzel, A.; Glasser, G.; Langner, A.; Müller, F.; Gösele, U.; Knoll, W.; Azzaroni, O. Hybrid Polymer−Silicon Proton Conducting Membranes via a Pore-Filling Surface-Initiated Polymerization Approach. *ACS Appl. Mater. Interfaces* **2010**, *2*, 279−287.

(34) Bayat, H.; Raoufi, M.; Zamrik, I.; Schönherr, H. Poly-(Diethylene Glycol Methylether Methacrylate) Brush-Functionalized Anodic Alumina Nanopores: Curvature-Dependent Polymerization Kinetics and Nanopore Filling. *Langmuir* **2020**, *36*, 2663−2672.

(35) León-Boigues, L.; von Bilderling, C.; Pietrasanta, L. I.; Azzaroni, O.; Giussi, J. M.; Mijangos, C. A Patterned Butyl Methacrylate-Co-2-Hydroxyethyl Acrylate Copolymer with Softening Surface and Swelling Capacity. *Polymers* **2019**, *11*, 290.

(36) Masuda, H.; Yada, K.; Osaka, A. Self-Ordering of Cell Configuration of Anodic Porous Alumina with Large-Size Pores in Phosphoric Acid Solution. *Jpn. J. Appl. Phys.* **1998**, *37*, L1340.

(37) Masuda, H.; Fukuda, K. Ordered Metal Nanohole Arrays Made by a Two-Step Replication of Honeycomb Structures of Anodic Alumina. *Science* **1995**, *268*, 1466−1468.

(38) Hutter, J. L.; Bechhoefer, J. Calibration of Atomic-force Microscope Tips. *Rev. Sci. Instrum.* **1993**, *64*, 1868−1873.

(39) Wang, H.-J.; Zhou, W.-H.; Yin, X.-F.; Zhuang, Z.-X.; Yang, H.-H.; Wang, X.-R. Template Synthesized Molecularly Imprinted Polymer Nanotube Membranes for Chemical Separations. *J. Am. Chem. Soc.* **2006**, *128*, 15954−15955.

(40) Allegretto, J. A.; Iborra, A.; Giussi, J. M.; Bilderling, C.; Ceolín, M.; Moya, S.; Azzaroni, O.; Rafti, M. Growth of ZIF-8 MOF Films with Tunable Porosity by Using Poly (1-Vinylimidazole) Brushes as 3D Primers. *Chem.—Eur. J.* **2020**, *26*, 12388−12396.

(41) Wackerly, J. W.; Dunne, J. F. Synthesis of Polystyrene and Molecular Weight Determination by 1H NMR End-Group Analysis. *J. Chem. Educ.* **2017**, *94*, 1790−1793.

(42) Dwyer, A. B.; Chambon, P.; Town, A.; He, T.; Owen, A.; Rannard, S. P. Is Methanol Really a Bad Solvent for Poly(n-Butyl Methacrylate)? Low Dispersity and High Molecular Weight Polymers of n-Butyl Methacrylate Synthesised via ATRP in Anhydrous Methanol. *Polym. Chem.* **2014**, *5*, 3608−3616.

(43) Gallardo, A.; Aguilar, M. R.; Abraham, G. A.; San Román, J. Chain Copolymerization Reactions: An Algorithm to Predict the Reaction Evolution with Conversion. *J. Chem. Educ.* **2004**, *81*, 1210−1215.

(44) Mayo, F. R.; Lewis, F. M. Copolymerization. I. A Basis for Comparing the Behavior of Monomers in Copolymerization; The Copolymerization of Styrene and Methyl Methacrylate. *J. Am. Chem. Soc.* **1944**, *66*, 1594−1601.

(45) Schier, J. E. S.; Hutchinson, R. A. The Influence of Hydrogen Bonding on Radical Chain-Growth Parameters for Butyl Methacrylate/2-Hydroxyethyl Acrylate Solution Copolymerization. *Polym. Chem.* **2016**, *7*, 4567−4574.

(46) Salsamendi, M.; Ballard, N.; Sanz, B.; Asua, J. M.; Mijangos, C. Polymerization Kinetics of a Fluorinated Monomer under Confinement in AAO Nanocavities. *RSC Adv.* **2015**, *5*, 19220−19228.

(47) Chyasnavichyus, M.; Young, S. L.; Tsukruk, V. V. Mapping Micromechanical Properties of Soft Polymer Contact Lenses. *Polymer* **2014**, *55*, 6091−6101.

(48) Salsamendi, M.; Ballard, N.; Sanz, B.; Asua, J. M.; Mijangos, C. Polymerization Kinetics of a Fluorinated Monomer under Confinement in AAO Nanocavities. *RSC Adv.* **2015**, *5*, 19220−19228.

(49) Ran, C.; Ding, G.; Liu, W.; Deng, Y.; Hou, W. Wetting on Nanoporous Alumina Surface: Transition between Wenzel and Cassie States Controlled by Surface Structure. *Langmuir* **2008**, *24*, 9952−9955.